IM465 – Conformação Plástica dos Metais – 2º semestre de 2011 – Quarto Artigo
Exercício de caráter estritamente individual. Envie-o para meu e-mail até 10/12/2011

O artigo a seguir apresenta um estudo sobre a conformabilidade a quente da liga Inconel 718. Responda as questões a seguir considerando o que foi apresentado no artigo e o que foi visto durante as aulas.

1) Quais os objetivos apresentados e como foram justificados? Os resultados obtidos permitem concluir que esses objetivos foram alcançados?

2) Descreva o procedimento experimental e associe-o aos objetivos apresentados.

3) Qual a justificativa metalúrgica para os autores terem ensaiado o material com tamanho de grão de 90 µm na faixa total de taxa de deformação?

4) Os resultados de tensão x deformação são coerentes com as condições de ensaio? Quais os mecanismos de encruamento e amaciamento presentes em cada condição apresentada nos gráficos?

5) Como os mapas de processamento foram elaborados? Como associar a potência dissipada com a conformabilidade a quente da liga metálica?

6) Identifique as regiões seguras e inseguras do mapa de processamento e associe-as às condições de ensaio e aos mecanismos que fizeram com que a liga se mantivesse contínua ou apresentasse defeitos.

7) Os resultados obtidos foram os esperados considerando-se a teoria sobre conformabilidade vista nas aulas?

Journal of Materials Processing Technology 211 (2011) 433–440

Contents lists available at ScienceDirect

Journal of Materials Processing Technology

journal homepage: www.elsevier.com/locate/jmatprotec

Processing map for hot working of Inconel 718 alloy

Feng-Li Sui[a,*], Li-Xia Xu[a], Li-Qing Chen[b], Xiang-Hua Liu[b]

[a] Anhui Key Laboratory of Materials and Processing, School of Materials Science and Engineering, Anhui University of Technology, No. 59 Hudong Road, Maanshan 243002, Anhui, China
[b] State Key Laboratory of Rolling and Automation, Northeastern University, 3-11 Wenhua Road, Shenyang 110004, Liaoning, China

ARTICLE INFO

Article history:
Received 18 January 2010
Received in revised form
21 September 2010
Accepted 24 October 2010

Keywords:
Inconel 718 alloy
Processing map
Dynamic recrystallization
Unstable region

ABSTRACT

Cylindrical specimens of Inconel 718 alloy with grain size of 90 μm were used in the compression tests and processing maps at the strains of 0.1, 0.3, 0.5 and 0.7 were developed at 950–1150 °C in the strain rate range 0.001–100 s^{-1}. Only one unstable region for adiabatic shear bands and one small dynamic recrystallization zone in the stable region are exhibited in the processing map at 0.1 strain. As the strain is beyond 0.3, there exist three unstable regions in the processing maps where one is for adiabatic shear bands and the other two are for intergranular cracking. At the same time, the zone of dynamic recrystallization with a peak efficiency of 0.39 at about 950 °C and 0.001 s^{-1} in the stable region is enlarged and the distribution of which is from lower temperature and lower strain rate to higher ones. Optical micrographs of the specimens compressed to 0.7 strain show good agreement with the processing maps and main hot working schedules have been designed. Influence of initial grain size from 10 μm to 90 μm on the occurrence temperature of adiabatic shear bands and intergranular cracking has been analyzed at a strain rate of 100 s^{-1} and in the temperature range 900–1200 °C.

1. Introduction

As a precipitation-strengthened Ni–Fe based superalloy, Inconel 718 is extensively used to manufacture critical parts in aeronautical, astronautical, oil and chemical industries due to its excellent mechanical, physical and anticorrosion behavior. The most advantage of this alloy is the microstructure and property can be controlled by deformation parameters adjustment. It has been widely accepted that a "processing map" is very beneficial for optimizing hot working processes and controlling microstructure without resorting to expensive and time-consuming trial-and-error methods. The processing map based on the theory of dynamic material model (DMM) was firstly developed by Prasad et al. (1984) to analyze the hot deformation behavior of Ti-6242 alloy and has become a powerful technology to analyze the hot-working process of materials. Safe and unsafe domains are identified in the processing map and various mechanisms are manifested as adiabatic shear band, flow localization, dynamic strain aging, intergranular cracking, mechanical twinning and kinking or flow rotations (Sagar, 2006; Wang et al., 2006, 2007) in the unsafe domain which should be avoided during hot deformation. Among the safe domains identified in a processing map, the domain of dynamic recrystallization is favored for hot working since the process of softening enhances the intrinsic workability. On the other hand, the processing map represents the efficiency of power dissipation under different temperatures and strain rates, which is directly related to the relative rate of entropy production in the system by the evolution of microstructure (Prasad, 2003).

Processing maps of Inconel 718 alloy were successively developed by Srinivasan and Prasad (1994), Narayana Murty and Nageswara Rao (1998, 1999), different calculation methods and criteria were adopted in their works. However, specimens used in their works before hot deformation exhibit fine-grained structure ($d \approx 7$ μm) and only the processing map at 0.5 strain in the steady stage was provided in their reports. In fact, the billet of Inconel 718 alloy for hot deformation is usually heated and exhibits coarse-grained structure, and it is necessary to use processing maps at different strains to analyze a deformation process, e.g. a rolling process.

In the present investigation, cylindrical specimens of Inconel 718 alloy with grain size of 90 μm were used in the compression tests and a series of true stress–true strain curves were obtained. The processing map at 0.7 strain was developed using the dynamic material model and areas defined for different deformation mechanisms were verified by microstructure observations of the deformed specimens. At last, deformation mechanism maps at strains of 0.1, 0.3, 0.5 and 0.7 were developed for a continuous deformation process. The hot plastic deformation behavior of Inconel 718 alloy has been studied and the influence of initial specimen grain size on these has been discussed.

* Corresponding author. Tel.: +86 555 2311045; fax: +86 555 2311045.
E-mail address: fenglisui@21cn.com (F.-L. Sui).

0924-0136/$ – see front matter © 2010 Elsevier B.V. All rights reserved.
doi:10.1016/j.jmatprotec.2010.10.015

2. Experimental procedures

Inconel 718 alloy having the following composition (in wt%) was used in this investigation: C-0.044, Si-0.13, Mn-0.10, Ni-52.61, Cr-18.98, Mo-3.05, Nb-5.14, Al-0.46, Ti-0.92 and Fe-balance. The specimens of ϕ8 mm × 12 mm were manufactured from the forged billets and treated at 1100 °C for 10 min, 20 min and 30 min, respectively. Optical micrographs corresponding to the untreated and the treated specimens are shown in Fig. 1a (the untreated, $d \approx 10\,\mu$m), Fig. 1b (1100 °C for 10 min, $d \approx 40\,\mu$m), Fig. 1c (1100 °C for 20 min, $d \approx 75\,\mu$m) and Fig. 1d (1100 °C for 30 min, $d \approx 90\,\mu$m).

The specimens of grain size 90 μm were chosen to be deformed on a Gleeble-3800 simulator in the temperature range 950–1150 °C at an interval of 50 °C and in the strain rate range 0.001–100 s^{-1}. At each temperature and strain rate, many tests were carried out in order to obtain the flow stress–strain curves with a confidence interval of ±5% at significance level of 0.05. The flow stress data were corrected for adiabatic temperature rise measured by inserting a thermocouple in the specimen during testing. The specimens with grain size of 10 μm, 40 μm, 75 μm and 90 μm were separately deformed at a strain rate of 100 s^{-1} and in the temperature range 900–1200 °C at an interval of 25 °C to analyze the influence of initial specimen grain size to hot plastic deformation behavior of Inconel 718 alloy. Tantalum foil of 0.1 mm thickness was used between the specimen and dies to avoid sticking of the specimen to the dies. All specimens were soaked for 180 s at the test temperatures described above, then deformed to a true strain of 0.7 and immediately water cooled to the room temperature. The deformed specimens were sectioned longitudinally (parallel to the compression axis) and the cut surface was prepared for metallographic examination using standard optical and scanning electron microscopy techniques.

3. Results and discussion

3.1. Stress–strain behavior

The specimens of grain size 90 μm were used in hot compression tests and the true stress–true strain curves are shown in Fig. 2 where a–f corresponds to the strain rates of 0.001 s^{-1}, 0.01 s^{-1}, 0.1 s^{-1}, 1 s^{-1}, 10 s^{-1} and 100 s^{-1}, 1–5 correspond to the temperatures of 950 °C, 1000 °C, 1050 °C, 1100 °C and 1150 °C. These curves represent typical strain hardening behavior and most of the curves show steady state region only as: (i) the strain rate is slower than 1 s^{-1}, (ii) the strain rate is 10 s^{-1} and the temperature is higher than 950 °C and (iii) the strain rate is 100 s^{-1} and the temperature is higher than 1000 °C.

3.2. Establishment of processing maps

The flow stress data obtained at different temperatures, strain rates and 0.7 strain are given in Table 1. A linear statistical regression method was used to analyze the relationship between $\log\sigma$ and $\log\dot{\varepsilon}$ and the result is shown in Fig. 3. The plot shows that very good correlation exists at temperatures from 1000 to 1100 °C, while the data at lower and higher temperatures (950 °C and 1150 °C) have shown some deviation. The one-dimensional linear correla-

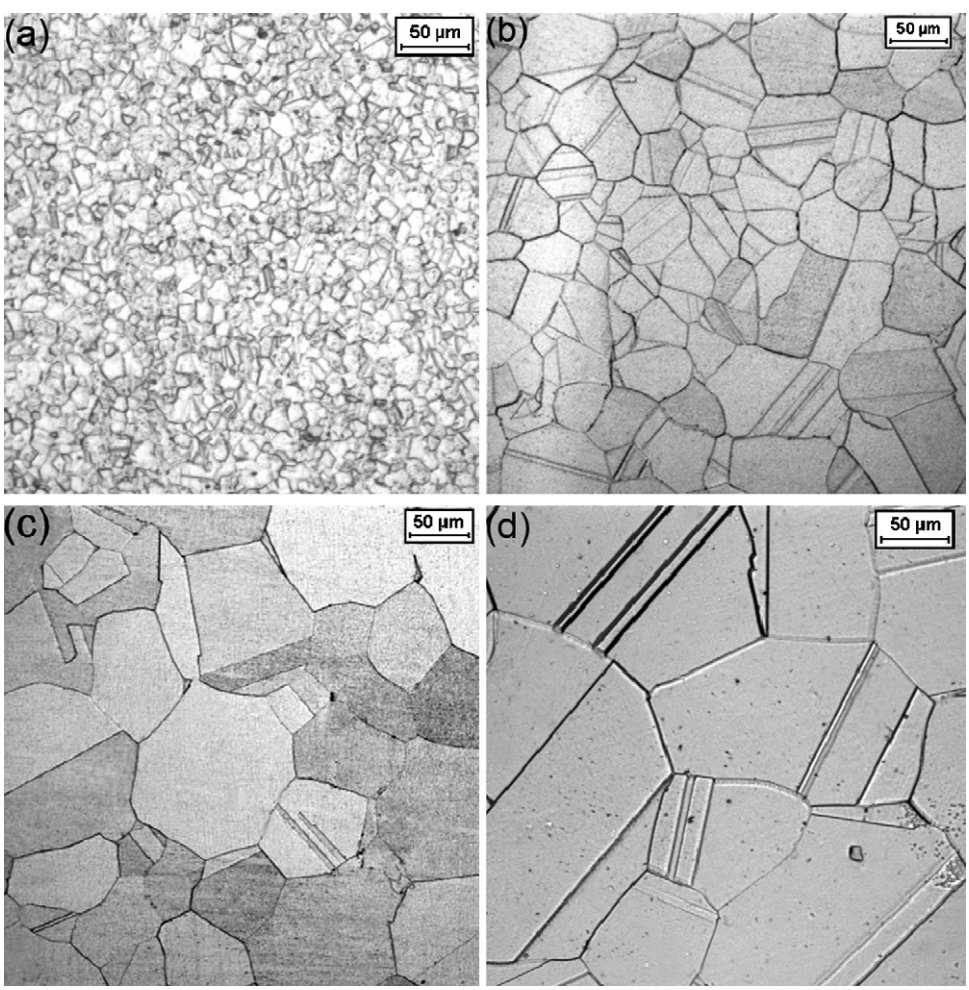

Fig. 1. Optical micrographs of Inconel 718 alloy before deformation.

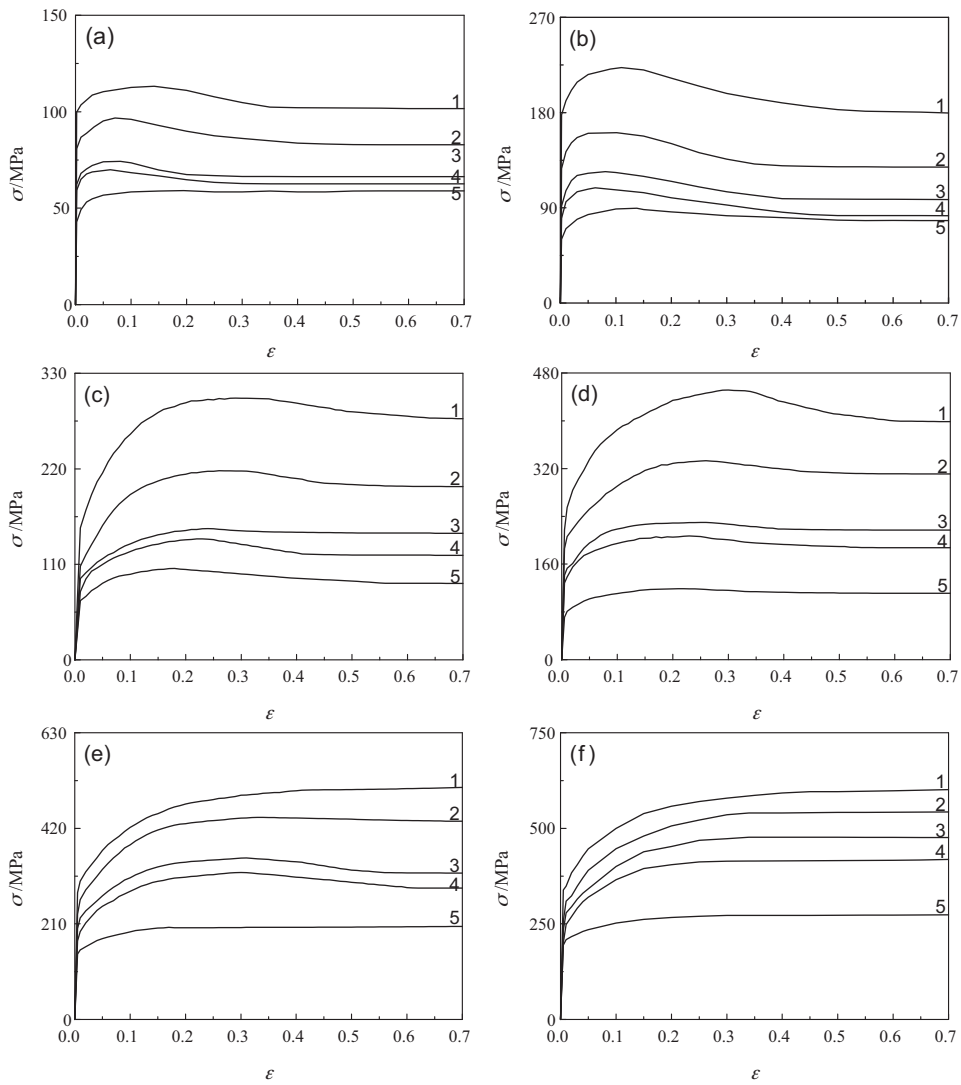

Fig. 2. True stress–true strain curves of Inconel 718 alloy.

tion coefficient is between 97.5671 and 99.8023%, which indicates that the linear relationship between $\log\sigma$ and $\log\dot{\varepsilon}$ is obvious and the flow behavior of Inconel 718 alloy obeys power-law (Eq. (1)). This means that the efficiency of power dissipation η and the instability parameter ξ at different strain rates and temperatures can be calculated from Eqs. (2)–(4) (Prasad et al., 1984; Prasad, 1990):

$$\sigma = K\dot{\varepsilon}\Big|_{\varepsilon,T} \tag{1}$$

$$m = \left[\frac{\partial \ln(\sigma)}{\partial \ln(\dot{\varepsilon})}\right]_{\varepsilon,T} \tag{2}$$

$$\eta = \frac{2m}{m+1} \tag{3}$$

$$\xi(\dot{\varepsilon}) = \frac{\delta \ln[m/m+1]}{\delta \ln \dot{\varepsilon} + m} \tag{4}$$

Table 1
Flow stress (in MPa) of Inconel 718 alloy at different strain rates, temperatures and 0.7 strain.

Strain rate (s^{-1})	Temperature (°C)				
	950	1000	1050	1100	1150
0.001	101.66	82.89	66.34	62.63	58.95
0.01	179.59	128.50	97.82	82.48	77.91
0.1	277.66	199.56	145.85	120.49	88.06
1.0	398.51	311.05	216.89	187.59	111.35
10.0	510.17	435.92	321.69	288.57	204.56
100.0	601.33	542.93	475.87	418.79	273.67

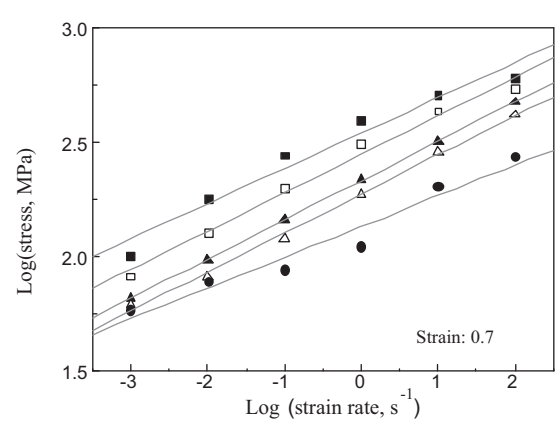

Fig. 3. Relationship between $\log\sigma$ and $\log\dot{\varepsilon}$ at 0.7 strain (■, 950 °C; □, 1000 °C; ▲, 1050 °C; △, 1100 °C; ●, 1150 °C).

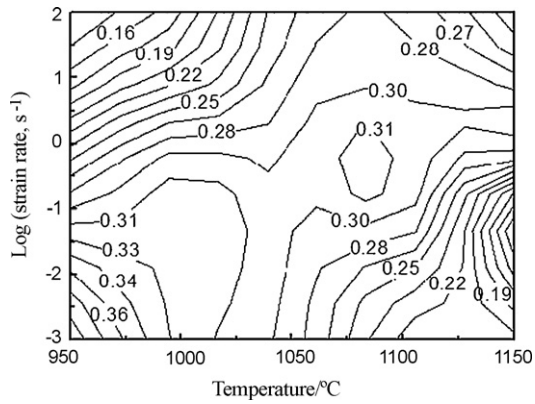

Fig. 4. Power dissipation map at 0.7 strain.

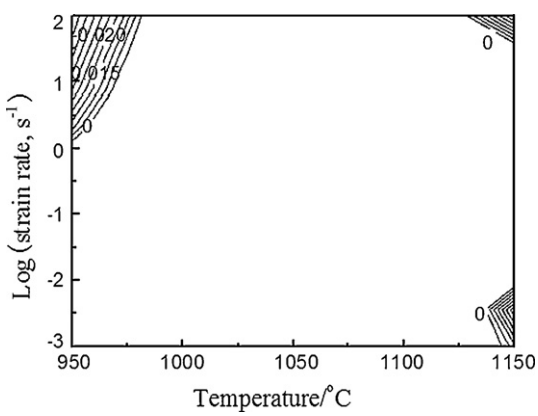

Fig. 5. Distribution of unstable deformation region ($\xi < 0$) at 0.7 strain.

The change of η with strain rate $\dot{\varepsilon}$ and deformation temperature constitutes a map called power dissipation map. The power dissipation map of Inconel 718 alloy at 0.7 strain is shown in Fig. 4 and the contour numbers in which represent the constant efficiency of power dissipation. The instability map can be generated by representing the variation of ξ with temperature and $\dot{\varepsilon}$ and the unstable regions in this map can be evaluated by using instable criterion $\xi < 0$ (proposed by Prasad, 1990). The instability map of Inconel 718 alloy at 0.7 strain is shown in Fig. 5. Finally, the processing map of Inconel 718 alloy at 0.7 strain (Fig. 6) for the specimens of grain size 90 μm was developed by superimposition of the power dissipation map in Fig. 4 and the instability map in Fig. 5.

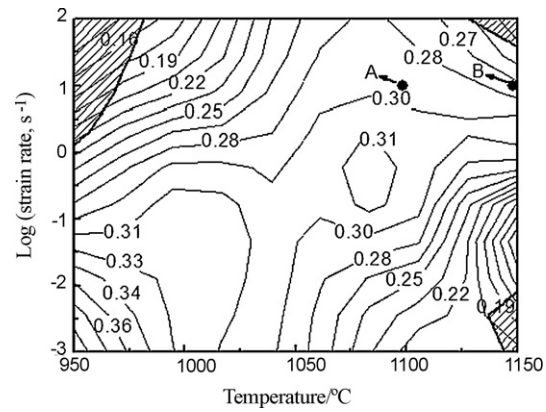

Fig. 6. Processing map of Inconel 718 alloy at 0.7 strain.

3.3. Definition of unstable regions

Three unstable regions displayed in Fig. 6 are evaluated using stability criteria and located in the positions of top left corner (950–960 °C, 1–100 s^{-1}), top right corner (1125–1150 °C, 30–100 s^{-1}) and lower right corner (1140–1150 °C, 0.001–0.01 s^{-1}).

Optical micrographs of the specimens deformed at 1150 °C, 100 s^{-1} and 1150 °C, 0.001 s^{-1} showing intergranular cracking are displayed in Fig. 7a and b. According to the viewpoints of Srinivasan and Prasad (1994), the cracks are caused by intergranular embrittlement at higher strain rate and higher temperature due to the existence of iron as well as coarse carbides at the grain boundaries in Inconel 718 alloy. Further analysis by SEM observation and EDS spectra indicates the precipitates found existing in the cracks and just at the grain boundaries are Nb-compounds (Fig. 8), which leads to the intergranular embrittlement and the intergranular cracking at 100 s^{-1} and 1150 °C. At 0.001 s^{-1} and 1150 °C, the grain boundary will be melted and weakened due to the long time exposure under higher temperature at slower deformation speed, which leads to the intergranular cracking in the end.

The adiabatic shear bands oriented at about 45° with respect to the compression axis are exhibited by the optical micrographs of the specimen deformed at 950 °C, 100 s^{-1} and shown in Fig. 9. The same phenomenon has also been found in compression tests of Ti-6242 alloy and interpreted as a result of flow localization at lower temperature and higher strain rate which is determined by performance of material itself under specific external conditions (Semiatin and Lahoti, 1982).

Therefore, three unstable regions are defined as the adiabatic shear bands (950–960 °C, 1–100 s^{-1}) and the intergranular cracking (1080–1150 °C, 10–100 s^{-1} and 1140–1150 °C, 0.001–0.01 s^{-1}). The stable region surrounded by which consisting of dynamic recovery,

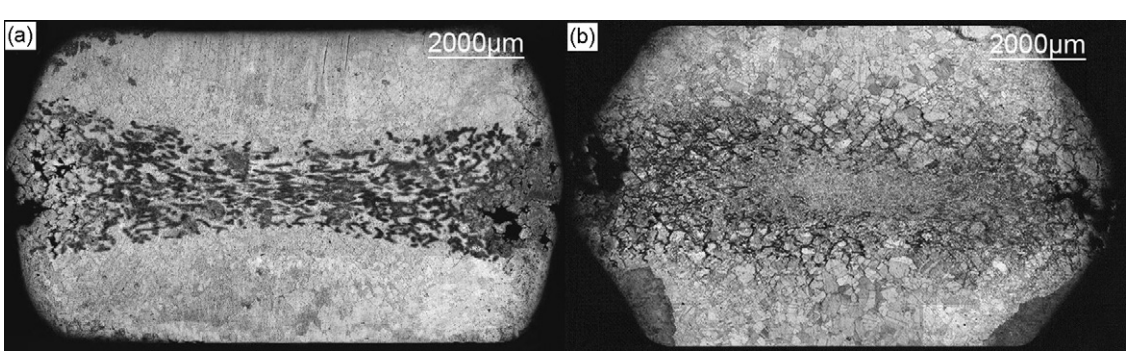

Fig. 7. Optical micrographs showing intergranular cracking at (a) 1150 °C, 0.001 s^{-1} and (b) 1150 °C, 100 s^{-1}.

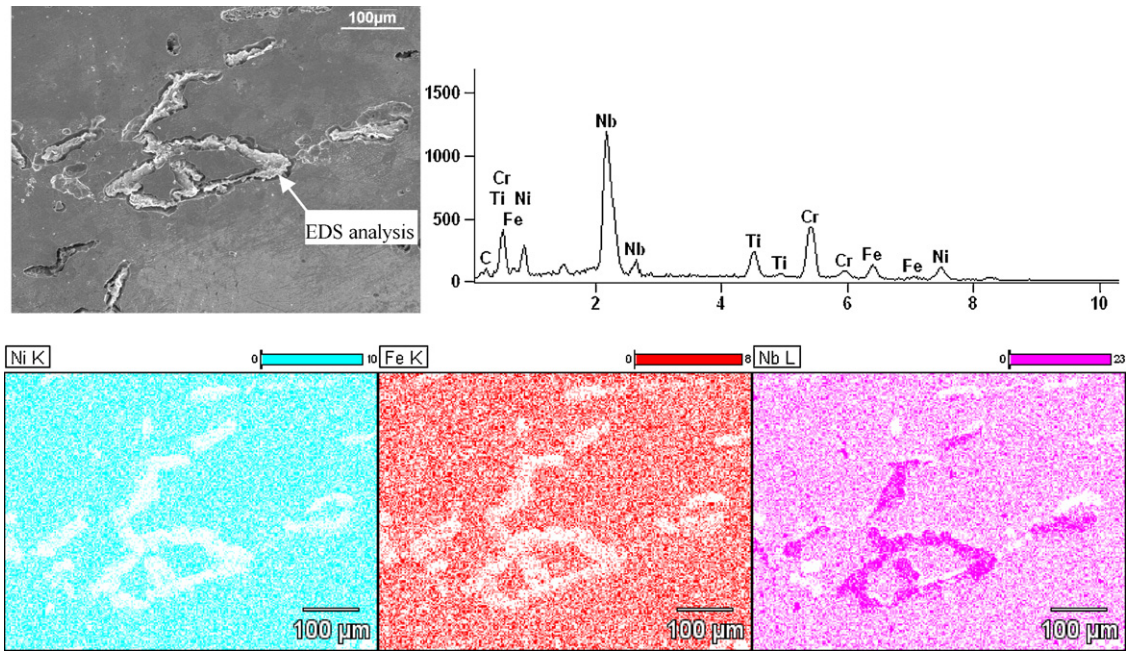

Fig. 8. SEM micrographs showing cracks with Nb compounds precipitates at the grain boundaries along with EDS and surface scanning at 1150 °C and 100 s^{-1}.

partial or fully dynamic recrystallization and dynamic recrystallization accompanied with grain growth will be discussed below.

3.4. Definition of dynamic recrystallization region

As a main feature, the stacking fault energy of Inconel 718 alloy is lower because of its face centered cubic structure. According to the viewpoints of Ravichandran and Prasad (1992), nucleation rate of austenitic grains in material with low stacking fault energy is lower since the dynamic recrystallization is controlled by it. Optical micrographs of the specimens deformed at 950 °C, 0.001 s^{-1} and 1100 °C, 10 s^{-1} showing dynamic recrystallization are displayed in Fig. 10a and b. Partial dynamic recrystallization or dynamic recovery is shown in Fig. 11. $\eta = 0.28$ can be regarded as the demarcation value of dynamic and partial dynamic recrystallization regions by the comparation between the points A and B marked in Fig. 6 corresponding to Figs. 10b and 11b. A dynamic recrystallization region with $\eta > 0.28$ is represented from lower strain rate and lower deformation temperature to higher ones in the stable region (Fig. 6). A peak efficiency of 0.39 occurs at about 950 °C and 0.001 s^{-1}, and the fine dynamic recrystallized grain is obtained (Fig. 10a). Obviously, the deviation of the data in Fig. 3 at 950 °C is just caused by the occurrence of dynamic recrystallization and adiabatic shear bands at the lower and higher strain rate, and which at 1150 °C is just caused by the occurrence of intergranular cracking. In the upper side of the stable region, two domains with $\eta < 0.28$ can be defined as partial dynamic recrystallization or dynamic recovery regions. Optical micrographs of specimens deformed at lower strain rate represent dynamic recrystallization accompanied with grain growth (Fig. 12) as the deformation temperature is more than 1020 °C which is caused by the long time exposure and the dissolution of δ phase due to high solid solubility of Nb atoms in matrix (Cai et al., 2003). So the domain with $\eta < 0.28$ in the lower right side of the stable region can be defined as the dynamic recrystallization accompanied with grain growth region.

3.5. Construction of deformation mechanism maps

Based on the above analysis, deformation mechanism maps for Inconel 718 alloy at the strains of 0.1, 0.3, 0.5 and 0.7 were developed and shown in Fig. 13. In which, the following zones are displayed: (1) the adiabatic shear bands, (2) the intergranular cracking, (3) the partial dynamic recrystallization or dynamic recovery, (4) the dynamic recrystallization accompanied with grain

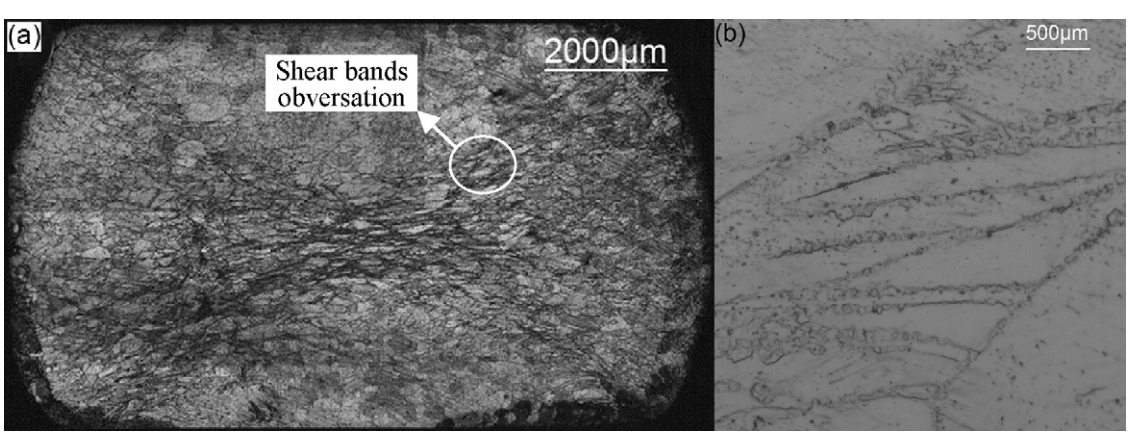

Fig. 9. Optical micrographs showing adiabatic shear bands at 950 °C, 100 s^{-1}.

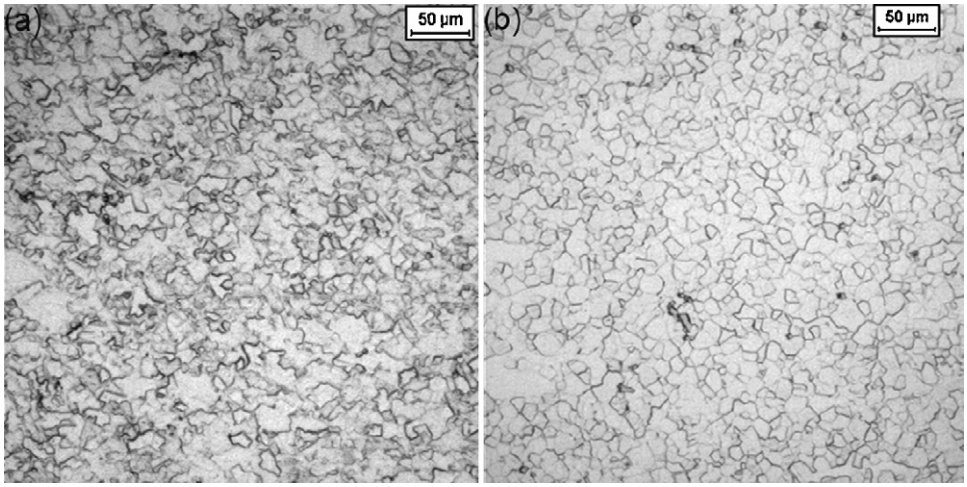

Fig. 10. Optical micrographs showing dynamic recrystallization at (a) 950 °C, 0.001 s^{-1} and (b) 1100 °C, 10 s^{-1}.

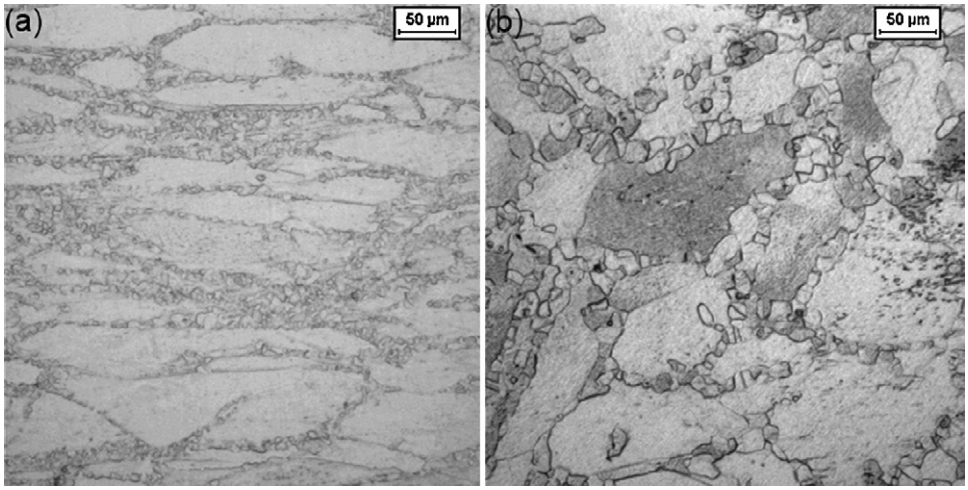

Fig. 11. Optical micrographs showing partial dynamic recrystallization at (a) 975 °C, 10 s^{-1} and (b) 1150 °C, 10 s^{-1}.

growth and (5) the dynamic recrystallization. With increasing the strain, the unstable regions change from one zone to three ones, the domain of dynamic recrystallization extends upward and rightward as the strain is lower than 0.5, the regime of dynamic recrystallization accompanied with grain growth is involved in the stable region from the strain of 0.3. The microstructure deformation mechanism maps become stable from the strain of 0.5, which has been verified in Ti–6Al–4V alloy (Park et al., 2002)

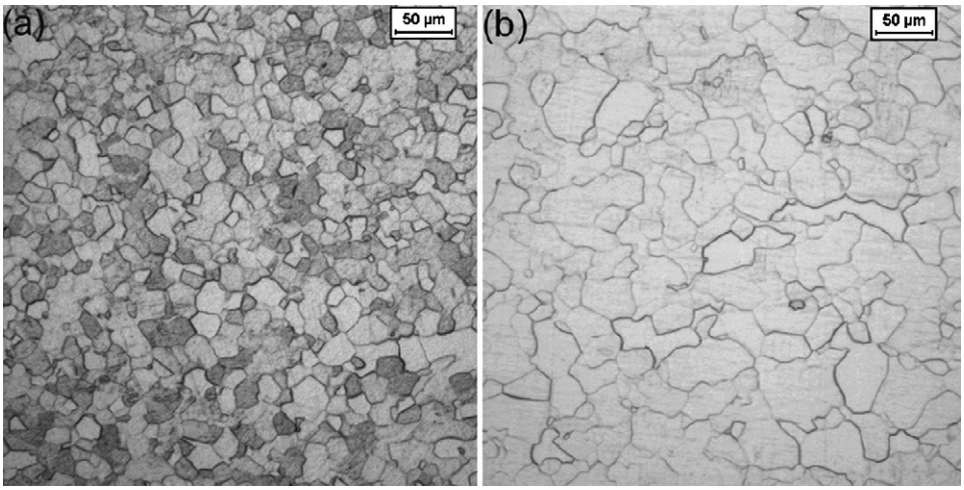

Fig. 12. Optical micrographs showing dynamic recrystallization accompanied with grain growth at (a) 1100 °C, 0.001 s^{-1} and (b) 1150 °C, 0.1 s^{-1}.

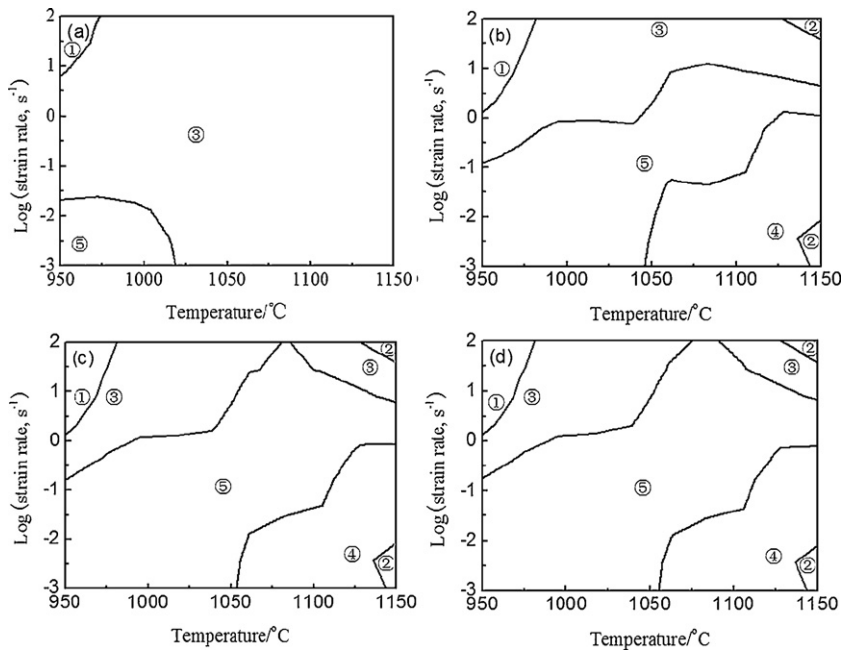

Fig. 13. Deformation mechanism maps for Inconel 718 alloy at strains of (a) 0.1; (b) 0.3; (c) 0.5; and (d) 0.7.

and Ni-based superalloy (Cai et al., 2007). Distribution trend of the dynamic recrystallization area in the deformation mechanism maps makes it possible to realize hot continuous rolling for Inconel 718 alloy considering the variation of temperature and strain rate in the workpiece during that process. During forging deformation, the temperature range 1050–1100 °C and strain rate range 0.05–30 s^{-1} can be chosen in blank production, the temperature range 950–1020 °C and strain rate range 0.001–0.5 s^{-1} can be chosen in final production and the peak efficiency region is an optimum condition for that process of this alloy.

3.6. Influence of initial grain size

Although the defects in Figs. 8 and 9 have been reported by Srinivasan and Prasad (1994), the deformation temperatures of which found in specimens are not 1150 °C and 950 °C but 1200 °C and 900 °C, which means the stable deformation region is narrowed for the coarsened alloy. At 100 s^{-1} strain rate, specimens exhibit different grain sizes of 10 μm, 40 μm, 75 μm and 90 μm were separately deformed in the temperature range 900–1200 °C at an interval of 25 °C. The occurrence temperatures of shear bands and intergranular cracking for specimens with different grain sizes are shown in Fig. 14 and those found by Srinivasan and Prasad (1994) are included. It can be seen the maximum occurrence temperature of the adiabatic shear bands is 950 °C and unchanged with the initial grain size in the designed tests. Obviously, the occurrence temperature 900 °C for the adiabatic shear bands found by Srinivasan and Prasad (1994) at 100 s^{-1} strain rate is not the maximum one. With the increase of initial grain size, the minimum occurrence temperature of intergranular cracking is reduced, and 1200 °C is the occurrence temperature of which as the grain size is 10 μm (even not more than 40 μm). As is known to us, strength of materials in high temperature is usually determined by the strength of grain boundary and generally described as Hall–Petch relation:

$$\sigma = \sigma_0 + K \cdot d^{-1/2} \tag{6}$$

where σ is the strength of materials and d is the diameter of grains. Therefore, the grain boundary can be strengthened by the refined grains due to the increased area of grain boundary and the cracking tendency will be reduced by which. In other words, deformation stability will be enhanced by the initial grain refinement and improved with the decrease of initial grain size for Inconel 718 alloy.

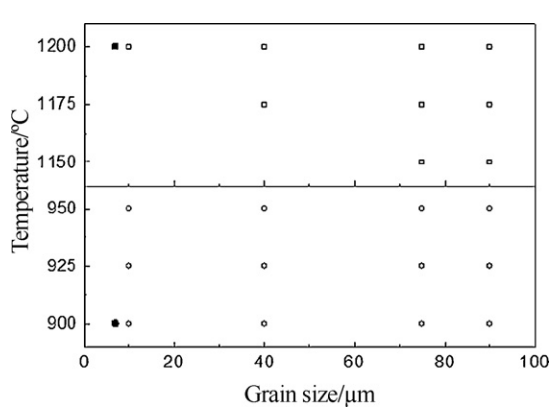

Fig. 14. Occurrence temperature of the adiabatic shear bands and intergranular cracking for specimens with different grain sizes deformed at 100 s^{-1} strain rate (○, adiabatic shear bands; □, intergranular cracking; ●, adiabatic shear bands and ■, intergranular cracking reported by Srinivasan and Prasad (1994)).

4. Conclusions

Processing maps of Inconel 718 alloy at the strains of 0.1, 0.3, 0.5 and 0.7 were developed using cylindrical specimens with grain size of 90 μm. Three unstable regions are presented in the processing map as the strain is not less than 0.3, where one is the region of shear bands located at 950–960 °C and 1–100 s^{-1} and the other two are regions of intergranular cracking located at 1125–1150 °C, 30–100 s^{-1} and 1140–1150 °C, 0.001–0.01 s^{-1}, respectively. The distribution of dynamic recrystallization zone in stable region is from lower temperature and lower strain rate to higher ones, and a peak efficiency of 0.39 occurs at about 950 °C and 0.001 s^{-1}. This distribution trend makes it possible to realize hot continuous rolling for Inconel 718 alloy considering the variation of temperature and strain rate in the workpiece during that process. During forging

deformation, the temperature range 1050–1100 °C and strain rate range 0.05–30 s^{-1} can be chosen in blank production, the temperature range 950–1020 °C and strain rate range 0.001–0.5 s^{-1} can be chosen in final production and the peak efficiency region is an optimum condition for that processing of this alloy.

Influence of initial grain size on the occurrence temperature of adiabatic shear bands and intergranular cracking has been analyzed by using specimens with the grain sizes of 10 μm, 40 μm, 75 μm and 90 μm at 100 s^{-1} strain rate, and those found by Srinivasan and Prasad (1994) using fine-grained specimens ($d \approx 6$ μm) were compared. With the increase of initial grain size, the maximum occurrence temperature of adiabatic shear bands is unchanged and the minimum occurrence temperature of intergranular cracking is reduced at that strain rate. As a result, the increase of initial grain size leads to the decrease of deformation stability.

Acknowledgements

The authors are grateful for the financial supports from the National Natural Science Foundation of China (Key Program, Grant No.: 50634030) and the Program for New Century Excellent Talents in University (Grant No.: NECT-06-0285).

References

Cai, D.Y., Zhang, W.D., Nie, P.L., et al., 2003. Dissolution kinetics and behavior of δ phase in Inconel 718. Trans. Nonferrous Met. Soc. China 13 (6), 1338.

Cai, D.Y., Xiong, L.Y., Liu, W.C., et al., 2007. Development of processing maps for a Ni-based superalloy. Mater. Charact. 58 (10), 941.

Narayana Murty, S.V.S., Nageswara Rao, B., 1998. On the development of instability criteria during hotworking with reference to IN718. Mater. Sci. Eng. A 254 (5), 76.

Narayana Murty, S.V.S., Nageswara Rao, B., 1999. On the flow localization concepts in the processing maps of IN718. Mater. Sci. Eng. A 267 (1), 159.

Park, N.K., Yeom, J.T., Na, Y.S., 2002. Characterization of deformation stability in hot forging of conventional Ti–6Al–4V using processing maps. J. Mater. Process. Technol. 130–131 (12), 540.

Prasad, Y.V.R.K., Gegel, H.L., Doraivelu, S.M., et al., 1984. Modeling of dynamic material behavior in hot deformation: forging of Ti-6242. Metall. Trans. A 15A (10), 1983.

Prasad, Y.V.R.K., 1990. Recent advance in the science of mechanical processing. Indian J. Technol. 28 (6–8), 435.

Prasad, Y.V.R.K., 2003. Processing maps: a status report. J. Mater. Eng. Perform. 12 (6), 638.

Ravichandran, N., Prasad, Y.V.R.K., 1992. Influence of oxygen on dynamic recrystallization during hot working of polycrystalline copper. Mater. Sci. Eng. A 156 (2), 195.

Sagar, P.K., 2006. Effect of alloying elements and microstructure on the processing parameters of α2 aluminide alloys. Mater. Sci. Eng. A 434 (1–2), 259.

Semiatin, S.L., Lahoti, G.D., 1982. The occurrence of shear bands in isothermal, hot forging. Metall. Trans. A 13A (2), 275.

Srinivasan, N., Prasad, Y.V.R.K., 1994. Microstructural control in hot working of IN-718 superalloy using processing map. Metall. Mater. Trans. A 25A (10), 2275.

Wang, C.Y., Wang, X.J., Chang, H., et al., 2007. Processing maps for hot working of ZK60 magnesium alloy. Mater. Sci. Eng. A 464 (1–2), 52.

Wang, W., Zhang, Y., Zeng, X., et al., 2006. Characterization of dynamic recrystallization in as-homogenized Mg–Zn–Y–Zr alloy using processing map. J. Mater. Sci. 41 (12), 3603.